Excited-State Dynamics of Hybrid Multichromophoric Systems: Toward an Excitation Wavelength Control of the Charge Separation Pathways

Natalie Banerji,[†] Guillaume Duvanel,[†] Alejandro Perez-Velasco,[‡] Santanu Maity,[‡] Naomi Sakai,[‡] Stefan Matile,*[,‡] and Eric Vauthey*[,†]

Department of Physical Chemistry and Department of Organic Chemistry, University of Geneva, 30 quai Ernest-Ansermet, CH-1211 Geneva 4, Switzerland

Received: April 18, 2009; Revised Manuscript Received: June 6, 2009

The photophysical properties of two hybrid multichromophoric systems consisting of an oligophenylethynyl (OPE) scaffold decorated by 10 red or blue naphthalene diimides (NDIs) have been investigated using femtosecond spectroscopy. Ultrafast charge separation was observed with both red and blue systems. However, the nature of the charge-separated state and its lifetime were found to differ substantially. For the red system, electron transfer occurs from the OPE scaffold to an NDI unit, independently of whether the OPE or an NDI is initially excited. However, charge separation upon OPE excitation is about 10 times faster, and takes place with a 100 fs time constant. The average lifetime of the ensuing charge-separated state amounts to about 650 ps. Charge separation in the blue system depends on which of the OPE scaffold or an NDI is excited. In the first case, an electron is transferred from the OPE to an NDI and the hole subsequently shifts to another NDI unit, whereas in the second case symmetry-breaking charge separation between two NDI units occurs. Although the charges are located on two NDIs in both cases, different recombination dynamics are observed. This is explained by the location of the ionic NDI moieties that depends on the charge separation pathway, hence on the excitation wavelength. The very different dynamics observed with red and blue systems can be accounted for by the oxidation potentials of the respective NDIs that are higher and lower than that of the OPE scaffold. Because of this, the relative energies of the two charge-separated states (hole on the OPE or an NDI) are inverted.

Introduction

Over the past few decades, considerable efforts have been invested in the design and the investigation of molecular systems mimicking the function of the photosynthetic apparatus of plants or bacteria.[1−19] Two major parameters have to be considered when conceiving efficient artificial photosynthetic systems: a high collection efficiency of light over most of the visible spectrum, and a sufficiently long-lived and energetic charge-separated state (CSS). The most common approach has been to imitate the natural photosynthetic organisms where light energy collection and charge separation (CS) are carried out in distinct units, the light-harvesting complexes and reaction centers, respectively.[20−22] Most artificial light-harvesting complexes elaborated so far are porphyrin arrays where the coupling between the chromophores is controlled by the length and the nature of the spacers.[1,23−30] Antenna systems based on other chromophores have also been reported,[9,31−37] with phenylethynyl dendrimeric systems being probably among the most promising.[38−40]

The most successful strategy for enhancing the lifetime of the CSS in artificial analogues of the reaction center has been the spatial separation of the charges through a cascade of secondary charge hopping following the initial photoinduced step. This approach is also inspired from the natural reaction centers where the electron is spatially separated from the hole upon successive hops to secondary accepting units. As a result, CS during several hundreds of microseconds or more has been realized at room temperature in triads, tetrads, and pentads.[1−4,13] However, multistep CS implies a free energy gradient and thus the energy stored in the final CSS represents, in many cases, a relatively small fraction of the initially absorbed photonic energy. Nevertheless, it should be noted that long-lived CS has recently been demonstrated in dyads where one of the constituents is a fullerene,[5] or a conjugated system,[6] allowing an extended delocalization of one of the charges. Finally, antenna−reaction center hybrids consisting of an array of chromophores covalently attached to a dyad have also been reported.[7−10]

An alternative to the above approach, which involves the synthesis of complicated macromolecular systems with a large number of covalently linked units, is supramolecular self-assembly.[11,12,14−19] Irradiation of self-assembled multichromophoric systems, consisting of eight blue core-substituted naphthalene diimides (NDIs) covalently attached to a *p*-octiphenyl (POP) scaffold, has recently been shown to lead to a transmembrane pH gradient, a crucial step in natural photosynthesis.[14,16] An original feature of these multichromophoric molecules is that they combine the functions of the antenna and of the reaction center.[41] Indeed, the large number of NDIs, eight in the individual molecule and 32 in the self-assembled transmembrane complex, ensures a high absorption cross section. Contrary to the natural photosynthetic apparatus, excitation is followed not by energy hopping toward the reaction center but rather by an ultrafast symmetry-breaking CS between two NDIs. The ensuing charges can either recombine or hop to a nearby neutral NDI, leading to a CSS lifetime that increases with the number of chromophores. The charge recombination (CR) time constant

* Corresponding authors. E-mail: Stefan.Matile@unige.ch (S.M.); Eric.Vauthey@unige.ch (E.V.).
[†] Department of Physical Chemistry.
[‡] Department of Organic Chemistry.

10.1021/jp903572r CCC: $40.75
Published on Web 07/01/2009

CHART 1: Structures of Hybrid Multichromophoric Systems[a]

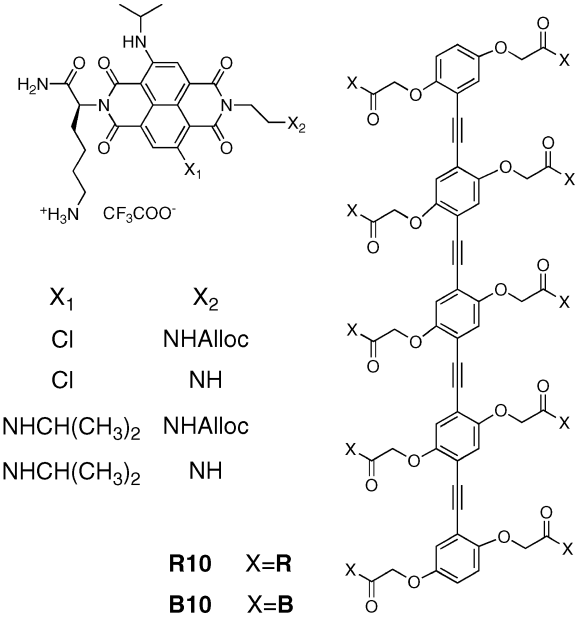

	X_1	X_2
R1	Cl	NHAlloc
R	Cl	NH
B1	$NHCH(CH_3)_2$	NHAlloc
B	$NHCH(CH_3)_2$	NH

R10 X=R
B10 X=B

[a] R and R1 consist in both 2,6- and 3,7-regio isomers; Alloc, allyloxycarbonyl.

was found to increase from 22 ps in a bichromophoric molecule, where hopping is not operative, to 45 ps in the octachromophoric system (B8) and to 400 ps in the transmembrane self-assembly. Furthermore, a spectacular increase of the CSS lifetime was observed upon going from blue to red NDIs (B and R in Chart 1), namely upon substitution of one the two amino core substituents by a chlorine atom. With such red NDI units, a CR component of about 1 ns was measured with the octachromophoric system (R8).[41] This slowing down cannot entirely be accounted for by the increase of driving force for CR of about 0.3 eV, associated with the different redox properties of blue and red NDIs. Instead, the occurrence of photoinduced CS between a red NDI and the POP scaffold, which is only energetically feasible with R8, could explain a longer-lived CSS as this process would lead to a better spatial confinement of the charges. Unfortunately, the existence of this additional CS pathway could not be evidenced spectroscopically, because of the strong overlap of the absorption spectra of the different ionic species in the visible region.

In order to further explore this idea of spatial charge confinement, with the perspective of realizing n-/p-heterojunctions, hybrid multichromophoric systems based on the same NDIs but with an oligophenylethynyl (OPE) chromophoric scaffold instead of a POP have been developed (Chart 1). The motivation to use OPE is threefold: (1) OPEs are known for their molecular wire properties,[42−44] and thus longer-lived CSS due to a better spatial separation of the charges could be expected; (2) the distance between two adjacent NDIs amounts to about 7−8 Å and is thus more favorable than POP for zipper-type assembly via π stacking;[17,18] (3) the OPE scaffold absorbs around 400 nm and can also take part in light harvesting.

We report here on our study of the excited-state dynamics of the two hybrid multichromophoric systems R10 and B10 (Chart 1) using femtosecond emission and absorption spectroscopies, upon excitation of either the OPE scaffold or an NDI unit. We will show that, although R10 and B10 are structurally very similar, their excited-state properties differ considerably. Moreover, these hybrid systems offer the possibility of a partial control of the CS pathways by the excitation wavelength.

Experimental Section

Samples. B1[14] and R1[18] were synthesized following previously reported procedures. The synthesis of R10 and B10 will be described in detail elsewhere. Selected data B10: RP-HPLC (Nucleosil 100-7 c18 250 × 8 mm, H_2O/(MeOH, 1% TFA) 1:9, 1 mL/min): t_R (min) 6.55; MS (MALDI): m/z (%) 6554 (100, $[M + H]^+$). Selected data R10: RP-HPLC (YMC-Pack ODS-A, 250 × 10 mm, H_2O/(MeOH, 1% TFA) 5:95, 1 mL/min): t_R (min) 4.65; MS (ESI, MeOH/CH_3CN/H_2O 4:3:1): 1606 (10, $[M + 4Na]^{4+}$), 1583 (15, $[M + 4H]^{4+}$), 1284 (25, $[M + 4Na + 1H]^{5+}$), 1267 (35, $[M + 5H]^{5+}$), 1071 (50, $[M + 4Na + 2H]^{6+}$), 1056 (75, $[M + 6H]^{6+}$), 918 (90, $[M + 4Na + 3H]^{7+}$), 905 (100, $[M + 7H]^{7+}$), 804 (55, $[M + 4Na + 4H]^{8+}$), 792 (65, $[M + 8H]^{8+}$). All measurements were performed in methanol (MeOH, spectroscopic grade). For steady-state and time-correlated single photon counting measurements, the concentration in terms of NDI units was on the order of 10 μM. For fluorescence up-conversion and transient absorption experiments, they amounted to about 1 mM and to 300 μM, respectively.

Steady-State Measurements. Absorption spectra were recorded on a Cary 50 spectrophotometer, whereas fluorescence and excitation spectra were measured on a Cary Eclipse fluorimeter. All fluorescence spectra were corrected for the wavelength-dependent sensitivity of the detection. For fluorescence measurements, the absorbance of the solutions at the band maximum was around 0.1 over 1 cm.

Time-Resolved Fluorescence. Fluorescence lifetime measurements on the nanosecond time scale were performed using the time-correlated single-photon-counting technique (TCSPC) as described in detail elsewhere.[45] Excitation was performed at 395 nm with a laser diode (Picoquant Model LDH-P-C-400B) generating ~60 ps pulses at 10 MHz. The instrument response function had a full-width at half-maximum (fwhm) of about 200 ps. The absorbance of the sample solutions at the excitation wavelength was about 0.1 over 1 cm.

Dynamics occurring on a shorter time scale was measured by fluorescence up-conversion as discussed before.[46] Excitation was achieved at 400 nm with the frequency-doubled output of a Kerr lens mode-locked Ti:sapphire laser (Tsunami, Spectra-Physics). Unless specified, the polarization of the pump pulses was at the magic angle relative to that of the gate pulses at 800 nm. For fluorescence polarization anisotropy measurements, the polarization of the pump pulse with respect to the gate pulse was controlled with a half-wave plate. The pump intensity on the sample was on the order of 5 $\mu J \cdot cm^{-2}$, and the fwhm of the instrument response function was ca. 210 fs. The sample solutions were located in a 0.4 mm rotating cell and had an absorbance of about 0.1 at 400 nm.

Transient Absorption (TA). The experimental setup was essentially the same as that described earlier,[47] except for the white-light probe pulses that were generated in a 3 mm CaF_2 plate, and for the detection that was achieved with a pair of 163 mm spectrographs (Andor Technology, SR163) equipped with a 512 × 58 pixel back-thinned CCD (Hamamatsu S07030-09) and assembled by Entwicklungsbüro Stresing, Berlin. Excitation was performed at 400 nm with the frequency-doubled output of a standard 1 kHz amplified Ti:sapphire system (Spectra-Physics) and at either 530 or 620 nm with a home-built two-stage noncollinear optical parametric amplifier. The pump intensity on the sample was ca. 1−2 $mJ \cdot cm^{-2}$. The polarization of the probe pulses was at the magic angle relative to that of the pump pulses. All spectra were corrected for the chirp of the white-light probe pulses. The fwhm of the response function was ca. 150 fs. The sample solutions were placed in a

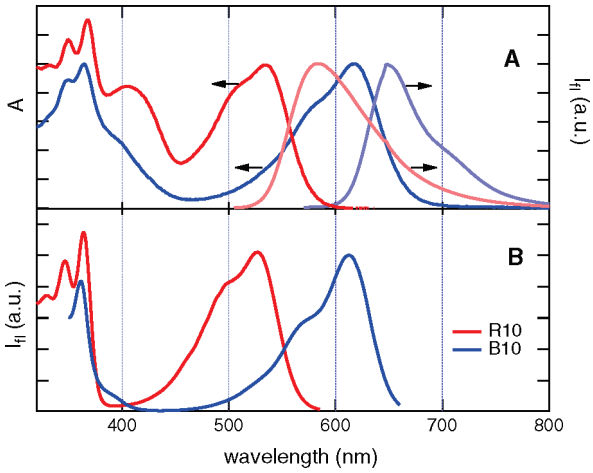

Figure 1. Absorption, fluorescence (local NDI excitation) (A), and fluorescence excitation spectra (B) of R10 and B10 in MeOH. The horizontal arrows designate the relevant vertical axis.

1 mm thick quartz cell and were continuously stirred by N_2 bubbling. Their absorbance at the excitation wavelength was around 0.3.

Results

Steady-State Spectra. The absorption spectra of R10 and B10 in MeOH exhibit several bands above 300 nm (Figure 1A). The first one at 530 nm for R10 and at 620 nm for B10 arises from the local NDI $S_0 \rightarrow S_1$ transition and will be designated here as the $S_0 \rightarrow$ NDI-LES transition (LES, local excited state). The energy of this charge-transfer type transition depends on the electron-donating property of the core substituents,[48] hence the difference of absorption maxima between R10 and B10. The second band that is more visible with R10 with a maximum around 410 nm is absent with the monomers, and can be undoubtedly assigned to the local OPE scaffold $S_0 \rightarrow S_1$ transition. This transition will be designated here as the $S_0 \rightarrow$ OPE-LES transition. Both the shape and location of this band are in excellent agreement with those reported for an alkoxy-substituted OPE of the same size.[49] The large width of the $S_0 \rightarrow S_1$ absorption band of OPEs is caused by an inhomogeneous broadening via torsional disorder.[50] The similar shape of the $S_0 \rightarrow$ OPE-LES bands points to torsional disorder in R10 and B10 as well. In B10, this band is not as distinct as in R10, because it is at a shorter wavelength and thus partially overlaps with the next absorption band. The latter is centered around 360 nm in both systems and exhibits a vibrational progression. This band is also present in the absorption spectra of core-unsubsituted NDIs, where it corresponds to the first electronic transition.[51−53] It can thus be assigned to a $\pi \rightarrow \pi^*$ transition involving only the NDI center, i.e., NDI without the core substituents.

The hypsochromic shift of the $S_0 \rightarrow$ OPE-LES band of B10 compared to R10 presumably originates from different OPE deplanarization by side chain repulsion. In general, free rotations around the formal single bonds between triple bonds and arenes of OPE produce numerous conformational isomers. Conformers with more coplanar arenes are better conjugated and exhibit higher conductivity and smaller band gaps.[54] Perpendicular orientation of adjacent arenes disrupts conjugation, lowers conductivity, and increases band gaps of OPE conformers. In B10, the OPE scaffold is deplanarized because intramolecular attraction between the weakly π-acidic, nonhalogenated NDIs fails to compensate charge repulsion between the side chains. The red-shifted absorption of R10 suggests that side chain attraction between strongly π-acidic, halogenated NDIs is sufficient to overcompensate charge repulsion. The validity of this interpretation was confirmed by OPE hypso- and bathochromism in response to complete side chain protonation and deprotonation, respectively. Detailed studies of pH-mediated OPE deplanarization in R10 and B10 are ongoing and will be reported in due course.

TABLE 1: Fluorescence Quantum Yields, Φ_{fl}, and Amplitude Average Lifetimes of the NDI-Centered Fluorescence, $\langle \tau_{fl} \rangle$

	Φ_{fl} (OPE-LES $\rightarrow S_0$)	Φ_{fl} (NDI-LES $\rightarrow S_0$)	$\langle \tau_{fl} \rangle$ (NDI-LES $\rightarrow S_0$) (ns)
R1[a]		0.08	2.3
R10 (λ_{ex} = 500 nm)		0.002	
R10 (λ_{ex} = 400 nm)	<0.001	0.001	0.019
B1[a]		0.32	8.4
B10 (λ_{ex} = 550 nm)		0.028	
B10 (λ_{ex} = 400 nm)	<0.001	0.008	0.013

[a] From ref 41.

Although all these bands can be easily assigned, the absorption spectra of R10 and B10 are not the composites of the spectra of the individual units. Indeed, the $S_0 \rightarrow$ NDI-LES bands are noticeably broader than those of R1 and B1 in the same solvent. This broadening is very similar to that observed with the octachromophoric systems, R8 and B8, where the scaffold is a POP.[41] This effect can be ascribed to an excitonic interaction between the chromophoric units. Given the torsional disorder associated with the OPE scaffold as well as the flexibility of the linkers, a rather broad distribution of distances and mutual orientations of the NDIs can be expected in both R10 and B10. This should in turn lead to a substantial distribution of excitonic interaction energies, hence to a broadening instead of a distinct splitting or shift of the absorption band.[55] Involvement of intermolecular aggregates can be safely ruled out as the absorption spectra were the same upon 5-fold dilution.

The fluorescence spectra of R10 and B10 upon local NDI excitation (Figure 1A) are very similar to those of R1 and B1 with maxima at 577 and 647 nm, respectively. However, the fluorescence quantum yield, Φ_{fl}, of the multichromophoric systems is reduced by more than a factor of 10 (Table 1). Excitation at 400 nm also results in NDI-centered (NDI-LES $\rightarrow S_0$) fluorescence but with a much smaller quantum yield. This indicates that, if excitation energy transfer between the OPE scaffold and the NDIs takes place, its efficiency, Φ_{EET}, is small. This is confirmed by the NDI-LES $\rightarrow S_0$ fluorescence excitation spectra of R10 and B10, which are very similar to those of R1 and B1, respectively, and present essentially no contribution from the $S_0 \rightarrow$ OPE-LES transition (Figure 1B). From these spectra, energy transfer efficiencies of less than about 0.05 can be estimated for both systems. The $S_0 \rightarrow$ NDI-LES band in the excitation spectra of R10 and B10 is narrower than in the absorption spectra. This points to the existence of a nonfluorescent subpopulation of excitonically coupled NDIs.

The fluorescence spectra of R10 and B10 upon 400 nm excitation exhibit a very weak feature between 450 and 520 nm that could be ascribed to OPE emission. This assignment is confirmed by the 450 nm fluorescence excitation spectra that are dominated by the broad $S_0 \rightarrow$ OPE-LES band. The intensity of this emission is so weak that only upper limit values of Φ_{fl} can be estimated (Table 1). OPEs are known to be strong fluorescers, with radiative rate constants, k_{rad}, on the order of 10^9 s^{-1},[49] and therefore the negligible OPE-LES $\rightarrow S_0$ fluores-

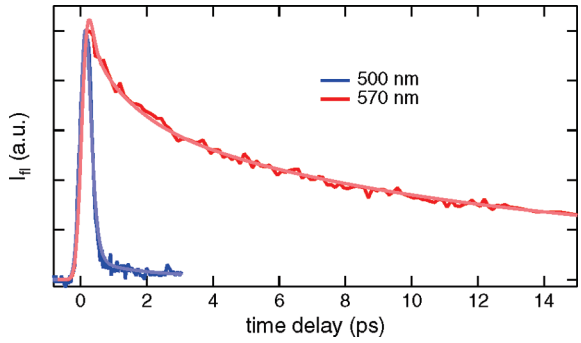

Figure 2. Time profiles of the fluorescence intensity measured with R10 at 500 and 570 nm upon 400 nm excitation and best multiexponential fits.

TABLE 2: Fluorescence Time Constants (with Relative Amplitudes) Obtained from the Up-Conversion Measurements upon 400 nm Excitation

	τ_{fl1} (ps)	τ_{fl2} (ps)	τ_{fl3} (ps)
R10 (λ_{fl} = 500 nm)	~0.06 (0.998)	1.4 (0.002)	
R10 (λ_{fl} = 570 nm)	1.3 (0.38)	9.8 (0.45)	86 (0.17)
B10 (λ_{fl} = 500 nm)	0.16 (0.99)	4.6 (0.01)	
B10 (λ_{fl} = 650 nm)	0.16 (−0.04)	4.6 (0.65)	28.1 (0.35)

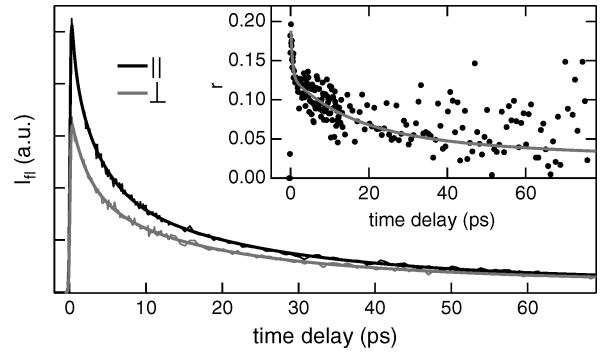

Figure 3. Time profiles of the polarized fluorescence and polarization anisotropy decay (inset) measured with R10 at 570 nm upon 400 nm excitation.

TABLE 3: Time Constants and Amplitudes Obtained from the Analysis of the Fluorescence Polarization Anisotropy Measured at the Band Maximum[a]

	τ_{r_1} (ps)	r_1	τ_{r_2} (ps)	r_2	τ_{r_3} (ps)	r_3	r_∞
R10	0.4	0.07	14.4	0.07	60	0.04	0.02
B10	0.6	0.05	24.6	0.05			0

[a] Relative error on the amplitudes is ±0.02.

cence, together with the small excitation energy transfer efficiencies, reveals the existence of another highly effective deactivation channel of the OPE-LES.

Time-Resolved Fluorescence. Fluorescence up-conversion measurements were performed upon 400 nm excitation only, and both OPE- and NDI-centered emissions were monitored (Figure 2). Emission at 500 nm, due mainly to the OPE-LES → S_0 transition, is extremely short-lived and is dominated by a decay component on the order of 100 fs, shorter than the instrument response function (Table 2). A slower component associated with a very small amplitude can also be observed. As its amplitude is larger with R10 than with B10, this component is assigned to the far blue edge of the NDI-centered emission.

As anticipated from the very small quantum yields, the NDI-centered fluorescence is also short-lived. The time profiles of this fluorescence measured at the band maximum of both systems need at least three exponential functions to be correctly reproduced. For R10, the three components correspond to decays, whereas for B10, the shorter time constant is associated with a rise of very small amplitude. For B10, the time constants listed in Table 2 have been obtained from global analysis of the fluorescence at 500 and 650 nm. It appears that the weak amplitude rising component of the NDI-centered fluorescence can be ascribed to an OPE-LES → NDI-LES transition, most probably through energy transfer, with the prompt rise being due to direct excitation of the NDIs at 400 nm. The weak amplitude of this component agrees with the small energy transfer efficiency deduced from the fluorescence excitation spectrum. Such an OPE-LES → NDI-LES transition cannot be observed in the fluorescence time profiles of R10, most probably because its amplitude is too small to result in a rise that can really be distinguished from the instrument response. Thus, most of the NDI-centered fluorescence upon 400 nm pumping arises from direct excitation of the NDI units. Finally, the time constants listed in Table 2 support our above assignment of the weak and slow component of the fluorescence at 500 nm to blue-edge NDI-centered emission.

Figure 3 presents the decay of the 570 nm fluorescence polarized in directions parallel, $I_{\parallel}(t)$, and perpendicular, $I_{\perp}(t)$, to the polarization of the pump light measured with R10. The temporal evolution of the fluorescence polarization anisotropy calculated as $r(t) = (I_{\parallel}(t) - I_{\perp}(t))/(I_{\parallel}(t) + 2I_{\perp}(t))$ is depicted in the inset. Not less than three exponential functions had to be used to reproduce $r(t)$, with the time constants and the amplitudes being listed in Table 3. On the other hand, the anisotropy decay measured with B10 could be reproduced with a biexponential function. Because excitation was performed far from the origin of the S_0 → NDI-LES transition, the initial anisotropy is substantially smaller than 0.4, the value expected for the case where the transition dipoles involved in the excitation and the emission are parallel. Because of this and of the relatively short fluorescence lifetime, the error on the anisotropy decay times and on their amplitude is large. Despite this, it is clear that the decay of the anisotropy is too fast to be attributed to the reorientation of an NDI unit. Indeed, the anisotropy decay time of R1 in MeOH amounts to 180 ps,[56] in good agreement with the reorientational motion of a molecule of this size.[57,58] Therefore, the fast anisotropy decay observed here with R10 and B10 can be attributed to the hopping of the excitation energy among the NDIs.

TA Measurements: R10, 400 nm Excitation. Figure 4A shows TA spectra measured with R10 in MeOH upon 400 nm excitation. These spectra consist of a broad positive band located between 450 nm and above 700 nm and a negative band below 450 nm. The positive band has a dip around 530 nm that can be ascribed to the bleach of the S_0 → NDI-LES absorption (Figure 1A). The spectrum above 450 nm is very similar to that of $R1^{\bullet-}$ generated upon photoinduced CS between R1 in the lowest singlet excited state and an electron donor.[41] On the other hand, the negative TA band below 450 nm coincides very well with the S_0 → OPE-LES absorption band and can be assigned to the bleach of this transition. These TA spectra present very small changes with time, except for the intensity that decays almost entirely to zero after about 1.5 ns. These spectra can be ascribed to a CSS, where the hole is on the OPE scaffold and the electron is on an NDI (OPE/NDI-CSS, Figure 5). The absorption spectrum of $OPE^{\bullet+}$ is not known but seems not to exhibit very specific features in the spectral window investigated. However, the involvement of the OPE scaffold in

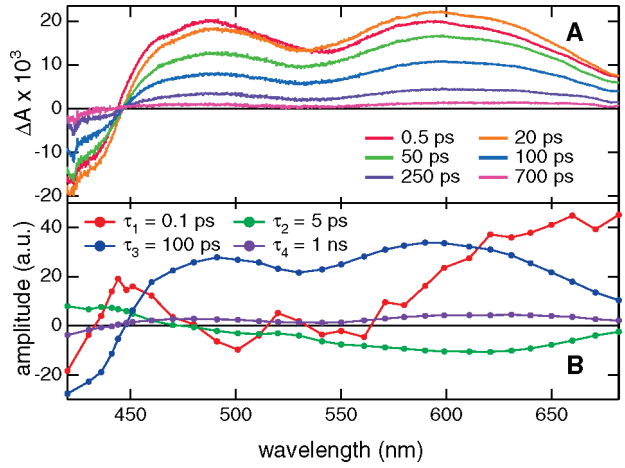

Figure 4. TA spectra recorded with R10 in MeOH upon 400 nm excitation (A) and decay associated spectra (B).

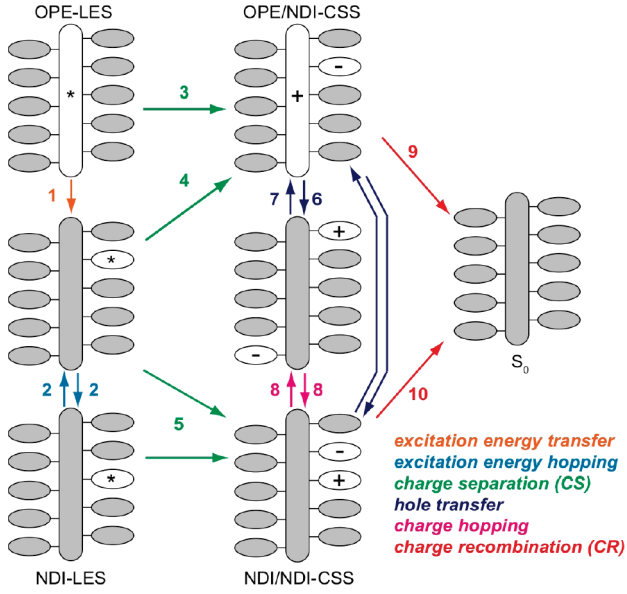

Figure 5. Schematic illustration of the various energy and charge transfer pathways in the multichromophoric systems.

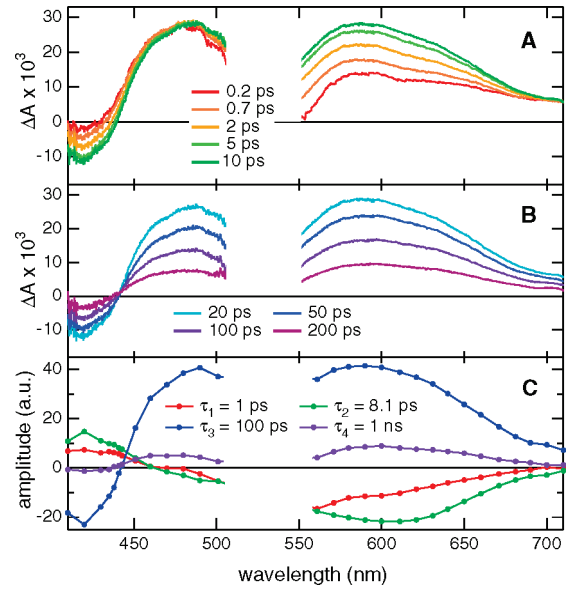

Figure 6. TA spectra recorded with R10 in MeOH upon 530 nm excitation (A, B) and decay associated spectra (C).

the CSS is confirmed by the bleach of the $S_0 \rightarrow$ OPE-LES transition below 450 nm that exhibits the same time dependence as the $NDI^{\bullet-}$ band.

The time profiles of the TA intensity over the whole spectral window were analyzed globally using the sum of four exponential functions, with the time constants listed in Table 4 and with the decay associated spectra depicted in Figure 4B. The shortest time constant is close to that measured by fluorescence at 500 nm and ascribed to the decay of the OPE-LES population. This time constant is assigned to CS between the excited OPE moiety and an NDI unit, resulting in the OPE/NDI-CSS (pathway 3 in Figure 5). In this case, the amplitude spectrum associated with this time constant should consist of the absorption spectrum of the OPE-LES (positive amplitude) minus that of the OPE/NDI-CSS (negative amplitude). This is in qualitative agreement with the observation, considering that the excited-state absorption spectrum of OPEs comprises a broad positive band ranging from about 500−550 nm to more than 700 nm.[49]

The amplitude spectrum associated with $\tau_2 = 5$ ps is very similar to the negative of the OPE/NDI-CSS spectrum. This time constant is thus assigned to the buildup of the OPE/NDI-CSS population as well, but upon direct excitation of the NDIs at 400 nm (pathway 4 in Figure 5). This interpretation is also supported by the positive value of the amplitude below 450 nm, pointing to a parallel increase of the $S_0 \rightarrow$ OPE-LES bleach. This positive amplitude is also probably associated with the NDI-LES, which has previously been shown to absorb between 400 and 500 nm.[41]

The spectra associated with the longest time constants, τ_3 and τ_4, are very similar and are essentially equal to the TA spectrum of the OPE/NDI-CSS. Therefore, these two time constants can be attributed to the decay of the OPE/NDI-CSS population back to the ground state upon CR (pathway 9 in Figure 5).

TA Measurements: R10, 530 nm Excitation. Whereas 400 nm pumping does not allow the OPE scaffold to be selectively excited, 530 nm pumping results in the exclusive excitation of the NDI units and should thus permit pathways 3 and 4 to the OPE/NDI-CSS to be disentangled. As illustrated in Figure 6A,B, the TA spectra recorded with R10 upon selective NDI excitation do not differ very much from those measured upon 400 nm pumping, especially after about 5 ps. At earlier time, however, the positive TA band in the 600 nm region is markedly smaller than that around 475 nm and the negative band below 450 nm,

TABLE 4: Time Constants Obtained from Global Analysis of the TA Data and Assignment[a]

	λ_{ex} (nm)	τ_1 (ps)	τ_2 (ps)	τ_3 (ps)	τ_4 (ns)	τ_{CSS}[b] (ns)
R10	400	0.10 (CS, 3)	5.0 (CS, 4)	100 (CR, 9)	1.0 (CR, 9)	0.65
R10	530	1.0 (CS, 4)	8.1 (CS, 4)	100 (CR, 9)	1.0 (CR, 9)	0.68
B10	400	0.25 (CS, 3)	4.0 (CS, 5)	43.5 (CR, 10)	3.0 (CR, 8 + 10)	2.7
B10	620	0.45 (CS, 5)	4.1 (CS, 5)	34.5 (CR, 10)	~5[c]	0.034

[a] The numbers in parentheses correspond to the pathway shown in Figure 5. [b] Intensity average CSS lifetime (see text). [c] Decay of a long-lived NDI-LES subpopulation (see text).

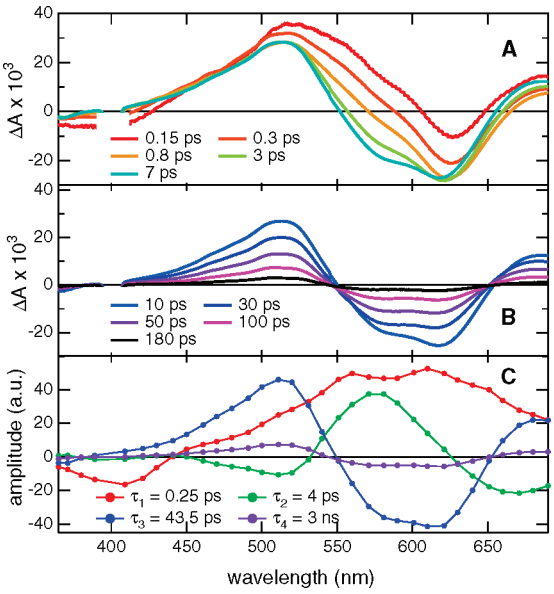

Figure 7. TA spectra recorded with B10 in MeOH upon 400 nm excitation (A, B) and decay associated spectra (C).

originating from the bleach of the $S_0 \rightarrow$ OPE-LES transition is very small. As time proceeds, both this bleach and the 600 nm band increase. After 5 ps, the spectral shape remains essentially constant and the TA intensity decays to zero within about 1.5 ns, as already observed upon 400 nm pumping. Global analysis of the time dependence of the TA intensity over the whole spectral window required four exponential functions, as before, with the time constants listed in Table 4, and the decay associated spectra depicted in Figure 6C. The spectra associated with the two fastest components, $\tau_1 = 1$ ps and $\tau_2 = 8.1$ ps, are quite similar in shape. Moreover, they resemble the spectrum associated with τ_2 found upon 400 nm pumping and ascribed to CS via pathway 4. This assignment is further supported here as these time constants account for the initial decrease of the relative intensity of the 475 nm TA band, a region where the NDI-LES has been shown to absorb.[41] Furthermore, the τ_1 and τ_2 values are very similar to the two shortest time constants found in the fluorescence decay of R10 (Table 3). Finally, the increase of the bleach below 450 nm reveals that the OPE scaffold is initially in its neutral ground state until CS takes place. Upon 400 nm pumping, this CS process was accounted for by a single exponential function with $\tau_2 = 5$ ps, while two exponentials are required here. This difference can be explained by the relatively small contribution of this pathway upon 400 nm excitation, because of the weak absorption coefficient of NDI at this wavelength. Detection of a biexponential dynamics would thus be hardly possible. It should be noted that the 5 ps time constant found with 400 nm pumping is close to the average of the 1 and 8.1 ps time constants.

The two largest time constants, τ_3 and τ_4, and their associated spectra are essentially identical to those observed upon 400 nm excitation. Therefore, these two time constants can be similarly assigned to CR via pathway 9.

TA Measurements: B10, 400 nm Excitation. The TA spectra recorded with B10 at several time delays after 400 nm excitation are presented in Figure 7A,B. During the first ~5−10 ps, the negative TA band below 450 nm evolves into a small dip centered around 365 nm, whereas that around 600 nm increases and broadens considerably. On the other hand, the positive TA band between 450 and 550 nm exhibits a substantial narrowing. From about 10 ps onward, the spectral shape remains almost constant and the whole TA intensity decays but does not totally vanish within the time window of the experiment. These late TA spectra are almost identical to those reported for B8 with a POP scaffold instead of an OPE,[14,41] and can be unambiguously ascribed to a CSS where both the hole and the electron reside on a different NDI unit (NDI/NDI-CSS). The TA spectra measured here with B10 reinforce further this assignment as the absence of the bleach of the $S_0 \rightarrow$ OPE-LES transition clearly demonstrates that the OPE scaffold is not involved in this CS. Indeed, the small negative dip at 365 nm is due to the bleach of the second NDI-centered transition. To get some insight into the pathways leading to the population of this NDI/NDI-CSS, a global analysis of the time evolution of the TA intensity was performed. As for R10, not less than four exponential functions were required; the resulting time constants are listed in Table 4 and the associated amplitude spectra are depicted in Figure 7C.

The spectra associated with the two largest time constants, τ_3 and τ_4, are essentially the same as the spectrum of the NDI/NDI-CSS. These time constants can consequently be related to CR along pathway 10 in Figure 5.

The τ_2-associated spectrum is quite similar to the negative of the NDI/NDI-CSS spectrum, indicating that this time constant should be related to CS. Furthermore, τ_2 is very close to τ_{fl2} measured by fluorescence up-conversion (Table 2), pointing to CS from the NDI-LES. Moreover, the TA spectrum of B1 in the S_1 state is characterized by a positive band around 575 nm,[41] in good agreement with the τ_2-associated spectrum. As a consequence, τ_2 can be unambiguously attributed to CS along pathway 5 (Figure 5).

The interpretation of the spectrum associated with τ_1 is less straightforward. It exhibits a negative band below 450 nm that can be interpreted as a bleach of the $S_0 \rightarrow$ OPE-LES transition and a broad positive band at longer wavelength that is similar to the excited-state absorption spectrum of OPE.[49] Thus, τ_1 can be undoubtedly ascribed to the decay of the OPE-LES population. In principle, two decay pathways can be envisaged: direct CS with an NDI to the OPE/NDI-CSS (pathway 3) and excitation energy transfer from the OPE scaffold to an NDI (pathway 1). The τ_1-associated spectrum does not really allow one of these processes to be excluded. However, as the fluorescence excitation spectrum of B10 points to energy transfer as a minor process, we ascribe τ_1 to CS along pathway 3.

TA Measurements: B10, 620 nm Excitation. The TA spectra recorded with B10 between about 2 and 200 ps after selective NDI excitation are very similar to those measured upon 400 nm pumping (Figure 8A,B). The earlier spectra exhibit a pronounced shoulder around 570 nm that can be unambiguously assigned to the absorption of the NDI-LES.[41] Moreover, the negative narrow TA band at short wavelength is due to the bleach of the second NDI-centered transition, whereas, upon 400 nm pumping, the broad negative band arises from the bleach of the OPE-centered transition. On the other hand, TA spectra after 200 ps are essentially the same as those measured with B1 alone and can thus be assigned to the NDI-LES. In this case again, four exponential functions were required for the global analysis of the TA time profiles, with the time constants listed in Table 4 and the amplitude spectra illustrated in Figure 8C. Many similarities can be found with those found upon 400 nm pumping (Figure 7C). The spectra associated with τ_3 are essentially identical and thus correspond to the same process, namely CR along pathway 10.

In the same way, the spectra found here for τ_1 and τ_2 are almost the same as the spectrum associated with τ_2 found with

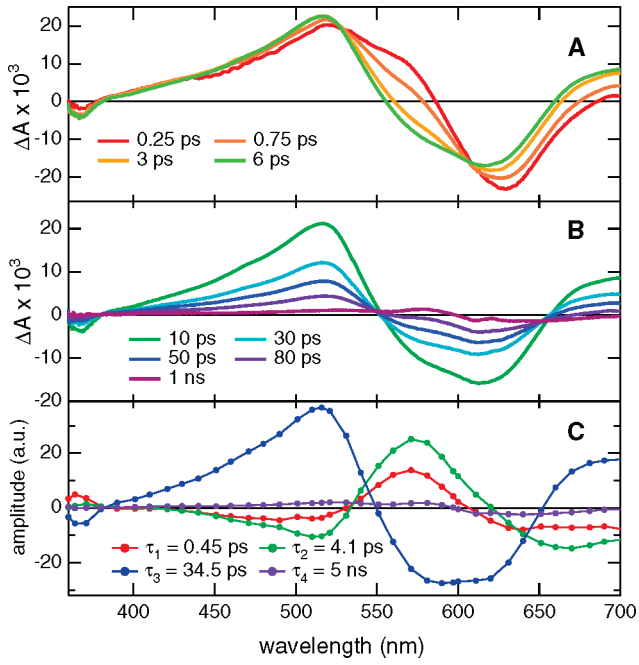

Figure 8. TA spectra recorded with B10 in MeOH upon 620 nm excitation (A, B) and decay associated spectra (C).

400 nm pumping. Thus, these two time constants can be similarly assigned to CS from NDI-LES to NDI/NDI-CSS (pathway 5). Finally, the spectrum associated with the largest time constant, τ_4, is identical to the late TA spectrum, ascribed to the NDI-LES. Therefore, this time constant can be interpreted as the decay of a long-lived population of this state.

Discussion

Excitation Energy Transfer. Two pathways for excitation energy transfer are in principle possible: energy transfer from the OPE scaffold to an NDI unit (pathway 1) and energy hopping between NDI units (pathway 2). All the results, namely the fluorescence excitation spectra, the fluorescence time profiles, and the TA data point to pathway 1 as a minor process compared to CS. On the other hand, the fluorescence polarization anisotropy measurements reveal that excitation energy hopping among NDI units is operative in both R10 and B10. The Förster radius for hopping among red and blue NDIs has been estimated to amount to 42 and 57 Å, respectively, assuming a random orientation of the energy donor and acceptors.[41] To have an estimate of the NDI−NDI distances, semiempirical quantum chemistry calculations have been performed with a molecule consisting of a biphenylethynyl scaffold with four NDIs similar to B1 but with all N-substituents replaced by H-atoms. In the resulting gas phase geometry, the center-to-center distance between the NDIs ranges from 8.2 to about 29 Å. On the other hand, the edge-to-edge distance can be as short as 2.3 Å. Considering the flexibility of the bridge linking the NDIs to the scaffold and the torsional disorder of the scaffold itself, many geometries, hence mutual orientations and distances between the NDIs, should be expected at room temperature. Therefore, the distances obtained from the calculations should only be considered as an estimate. Using the above-mentioned Förster radii, energy hopping between two NDIs at 8.2 Å is predicted to occur with a time constant, τ_{EEH}, on the order of 100 fs. This very small time constant together with the short interchromophoric distance points to a rather strong interaction between adjacent NDIs. The broadening of the $S_0 \rightarrow$ NDI-LES absorption band confirms substantial excitonic interaction. Consequently, the use of Förster theory, which is based on the point dipole approximation and presupposes weak interaction, is questionable. Despite this, it appears that energy hopping should be regarded as a major process in R10 and B10. The ultrafast polarization anisotropy decays measured with these two molecules (Figure 3) can thus be undoubtedly attributed to this process (pathway 2). The relationship between the anisotropy decay and τ_{EEH} depends on the number of chromophores, N, toward which excitation can hop from the initially excited one:[24,29]

$$r(t) = A(t) + B\exp(-(N+1)t/\tau_{EEH}) \quad (1)$$

where B, the loss of anisotropy due to the hopping of the excitation energy, depends on the mutual orientation of the NDIs, and where $A(t)$, the residual anisotropy, decays by reorientational motion of the emitters. According to the quantum chemistry calculations, the dihedral angle between two neighbor phenyl rings of the scaffold is on the order of 40°. Consequently, the four NDI units located at the ends of the scaffold have only one close neighbor, whereas the other six have two. According to Table 3, the fastest energy hopping processes in these systems should thus take place with a time constant on the order of 1 ps, assuming that no faster decay component of the polarization anisotropy has been missed. On the other hand, the slower anisotropy decay components might be associated with energy hopping to NDI units located on the other side of the scaffold. Such hopping can be expected to further reduce the fluorescence polarization.

Charge Separation Pathways. The TA data reveal that mostly the same CSS is populated independently of whether the OPE scaffold or an NDI is initially excited. However, the nature of this state differs for R10 and B10. This difference is related to the location of the hole: on the OPE scaffold in R10 and on an NDI in B10. As discussed in more detail below, this dissimilarity is probably at the origin of their distinct lifetimes.

The feasibility of photoinduced CS can be estimated by considering its driving force:[59]

$$\Delta G_{CS} = -E_{LES} - E_{red}(A) + E_{ox}(D) = -E_{LES} + E_{CSS} \quad (2)$$

where E_{LES} and E_{CSS} are the energies of the LES and of the CSS, respectively, and $E_{red}(A)$ and $E_{ox}(D)$ are the reduction and oxidation potentials of the electron acceptor and donor. The correction factor that accounts for the electrostatic interaction between the ionic moieties has been neglected here as it is generally accepted to be very small in polar solvents. The driving forces for the different CS pathways presented in Figure 5 are listed in Table 5. The $E_{NDI\text{-}LES}$ and the redox values of the NDI units have been taken from refs 18 and 41. The $E_{OPE\text{-}LES}$ can in principle be calculated from the average energy of the respective absorption and emission maxima. As no clear OPE-centered fluorescence can be detected with either R10 or B10, their emission maximum was estimated by considering that the Stokes shift of the emission band relative to the absorption band was the same as that observed with an alkoxy-substituted OPE of the same length.[49] These values have also been used to draw the energy level schemes depicted in Figure 9. These schemes strongly support the interpretation of the TA spectra. In the case of R10, excitation of the OPE scaffold is followed by essentially quantitative CS with an NDI unit (pathway 3). If energy transfer

TABLE 5: CSS Energies and Driving Forces for Photoinduced CS[a] Calculated Using eq 2

	CSS	E_{CSS} (eV)	ΔG_{CS}[b] (eV)
R10	OPE/NDI	1.94	−0.94 via OPE-LES (3)
			−0.39 via NDI-LES (4)
R10	NDI/NDI	2.25	−0.08 (5)
B10	OPE/NDI	2.03	−1.00 via OPE-LES (3)
			+0.03 via NDI-LES (4)
B10	NDI/NDI	1.95	−0.05 (5)

[a] Calculated with $E_{OPE\text{-}LES}(R10) = 2.88$ eV, $E_{OPE\text{-}LES}(B10) = 3.03$ eV, $E_{NDI\text{-}LES}(R10) = 2.33$ eV, $E_{NDI\text{-}LES}(B10) = 2.0$ eV, $E_{ox}(OPE) = 1.22$ V,[62] $E_{red}(R1) = -0.72$ V, $E_{ox}(R1) = 1.53$ V, $E_{red}(B1) = -0.81$ V, and $E_{ox}(B1) = 1.14$ V (all potentials are vs SCE and, if not specified, taken from ref 18). [b] The numbers in parentheses correspond to the pathway shown in Figure 5.

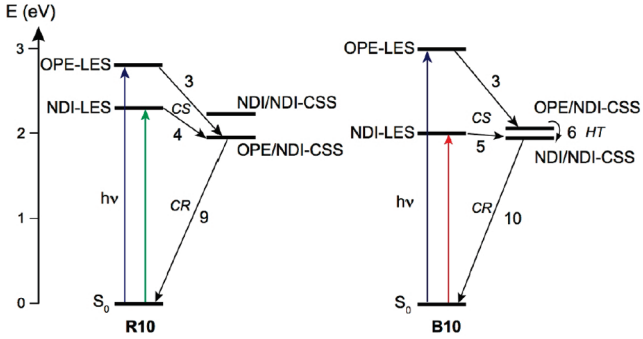

Figure 9. Energy level schemes pertaining to the relevant CS and CR processes in R10 and B10 (the numbers on the arrows correspond to the pathways shown in Figure 5).

to an NDI (pathway 1) takes place, it is only a minor pathway as discussed above. In the same way, excitation of an NDI also results in the same CSS via pathway 4. In principle, CS to the NDI/NDI-CSS (pathway 5) should be energetically possible. Spectroelectrochemical measurements reveal that the absorption spectra of $NDI^{\bullet+}$ and $NDI^{\bullet-}$ in the 400−700 nm region are very similar.[60] Despite this, the TA spectra of the NDI/NDI-CSS and of the OPE/NDI-CSS can be distinguished by the presence of the bleach of the OPE transition below 450 nm. As the TA time profile in this region is essentially the same as in the region where both $NDI^{\bullet+}$ and $NDI^{\bullet-}$ absorb, it can be concluded that either CS along pathway 5 is not competitive relative to CS along pathway 4 or that, if it takes place, it is followed by a much faster NDI/NDI-CSS → OPE/NDI-CSS transition. The latter process consists in a hole transfer from $NDI^{\bullet+}$ to the OPE (pathway 7). However, there is no reason why this hole transfer should be faster than CS along pathway 4. Therefore, the latter process is the most plausible origin of OPE/NDI-CSS population upon 530 mm pumping.

Table 4 shows that, upon 530 excitation of R10, CS along pathway 4 is characterized by two time constants of 1 and 8.1 ps. This apparent biexponential CS dynamics most probably reflects a distribution of CS time constants due to a distribution of the relative orientations of the NDIs relative to the OPE scaffold. It is indeed known that a Gaussian distribution of decay times can also be reproduced by a biexponential function.[61]

Table 4 also reveals that CS along pathway 3, with excitation on the OPE, is faster by a factor of at least 10 than CS along pathway 4 with excitation on an NDI. This large difference can be accounted for by at least two factors:

(1) CS via pathway 3 is more exergonic by about 0.5 eV (Table 5). Given the moderate ΔG_{CS} values, the rate constant can be expected to increase with increasing driving force, as predicted by Marcus electron transfer theory for the normal regime.[63]

(2) CS along pathway 3 depends on the overlap of the HOMO of the OPE with the LUMOs of all NDIs, as all 10 NDI units can act as quenchers of the OPE-LES. On the other hand, CS along pathway 4 depends on the overlap of the LUMO of the OPE with the HOMO of the excited NDI unit. Consequently, the electronic coupling constant, V_{CS}, for the first CS can be expected to be much larger than that for CS along pathway 4. Alternatively, one can consider that if excitation is on the OPE scaffold, there are 10 potential electron acceptors, whereas when excitation is on an NDI, there is only a single electron acceptor. Based on this, CS upon OPE excitation should be approximately 10 times faster than CS upon NDI excitation.

The situation is different for B10, as the main CS product is clearly an NDI/NDI-CSS. Upon 620 nm pumping, this state is the only accessible CSS. Indeed, no bleach of the $S_0 \rightarrow$ OPE-LES transition below 450 nm, which is characteristic of the TA spectrum of the OPE/NDI-CSS, can be observed. Moreover, according to eq 2, CS to the OPE/NDI-CSS should be endergonic (Table 5). The biexponential dynamics found for CS via pathway 5 can be explained by a distribution of time constants due to a distribution of mutual NDI/NDI orientations, as discussed above for R10. The CS time constants found are very short considering the relatively weak driving force of this process (Table 5). As already discussed in detail for B8,[41] this ultrafast CS could be ascribed to strongly coupled NDIs. The observation that the $S_0 \rightarrow$ NDI-LES absorption band of R10 and B10 differ from that of the single NDI units, while the fluorescence excitation spectra are identical, points to the existence of a nonemitting subpopulation. This subpopulation may be associated with geometries where two chromophores are sufficiently coupled to lead to a delocalization of the electronic excitation and thus to excitonic splitting.[55] The radiative rate constant also strongly depends on this relative orientation and totally vanishes in a H-dimer where the chromophores have a cofacial arrangement. However in the present case, even if the relative geometry of the chromophores is not that of a nonemitting H-dimer, the fluorescence is prevented by ultrafast CS. The geometries where the chromophores are far apart and that where they form a dimer most probably correspond to the extreme limits of a broad distribution of mutual orientations. Ultrafast symmetry-breaking CS process has also been observed upon excitation of bichromophoric perylene mono- and diimide dimers,[64] and of π-stacked perylene diimides.[32,65]

On the other hand, the NDI/NDI-CSS cannot be directly populated from the OPE-LES upon 400 nm pumping as this would require simultaneous electron and hole transfers from the OPE to two NDI units. Therefore, as excitation energy transfer from the OPE scaffold to an NDI unit (pathway 1) is negligible, the NDI/NDI-CSS should be populated via CS to the OPE/NDI-CSS (pathway 3) followed by hole transfer (pathway 6). Although the driving force for this transfer is small, $\Delta G_{HT} = -0.08$ eV, this process must be very fast, as testified by the very rapid disappearance of the $S_0 \rightarrow$ OPE-LES bleach (Figure 7A). This can be explained using a similar argument as for CS via pathway 3, namely by considering that the hole, initially located on the OPE, can move to all nine neutral NDI units. In this case as well, the electronic coupling, V_{HT}, is very large, because it depends on the overlap of the OPE HOMO with the LUMO of all nine NDIs. The exact time scale of this

process cannot be determined from our data, but it should be close to the value of 0.25 ps found for τ_1.

In the NDI/NDI-CSS generated along pathway 5, the two opposite charges should be on two adjacent NDIs. This is no longer true with the NDI/NDI-CSS populated via pathway 6 as, in this case, the opposite charges can be located on two very remote NDIs. This difference should have a strong repercussion on the lifetime of this state as discussed in more detail below.

Finally, the residual NDI-LES population observed in the TA spectra of B10 upon 620 nm pumping is ascribed to excited NDIs, most probably located at one end of the OPE scaffold, that have no close enough neighbor to undergo CS. Given the small amplitude of this contribution, this must correspond to a very minor fraction of the NDIs.

In conclusion, the different CS pathways in R10 and B10 can be entirely accounted for by energetic considerations, with the oxidation potentials of the red and blue NDI being lower and higher respectively than the oxidation potential of the OPE scaffold.

CS upon NDI excitation (pathways 4 and 5) and energy hopping occur on similar time scales. Therefore, excitation does not have the possibility to hop over many NDI units before CS takes place. Exciton annihilation can be a major deactivation pathway of excited states in aggregates and in multichromophoric systems.[29,66] This process manifests by a decrease of the fluorescence quantum yield with increasing excitation intensity. However as already discussed in detail elsewhere for R8 and B8,[41] the lifetime of the excitation in R10 and B10 is too short for this process to be very significant. This is supported by the similarity of the time constants obtained by the fluorescence up-conversion and TA techniques, where very different excitation intensities are used.

Charge Recombination. The CR dynamics in R10 and B10 contrast strongly by their time scales. In order to better compare them, values of the intensity average CSS lifetime, $\bar{\tau}_{CSS}$, defined as $\bar{\tau} = \sum_i f_i\tau_i$ with $f_i = a_i\tau_i/\sum_i a_i\tau_i$, are listed in Table 4. This intensity average lifetime is better suited than the amplitude average lifetime, $\langle\tau\rangle = \sum_i a_i\tau_i$ with $\sum_i a_i = 1$, to account for an average population decay.[67,68] On the other hand, the amplitude average lifetime, as used in Table 1, is useful when comparing fluorescence quantum yields.[67,68]

The origin of this difference lies in the nature of the charge-separated state: OPE/NDI-CSS for R10 and NDI/NDI-CSS for B10. In R10, the hole and electron are confined in distinct parts of the molecule, namely the OPE scaffold and the NDIs, respectively. The hole should be delocalized over the whole scaffold, whereas the electron can in principle hop to adjacent NDI units (pathway 8 in Figure 5). In this respect, R10 can be considered as a molecular n-/p-heterojunction. The biexponential CR dynamics in this system most probably reflects a distribution of CR time constants due to a distribution of the mutual OPE/NDI orientations as discussed above for CS. Table 5 and Figure 9 show that the driving forces for CR, $\Delta G_{CR} \approx E_{CSS}$, along pathway 9 in R10 and along pathway 10 in B10 are essentially the same. The longer lifetime of the red OPE/NDI-CSS can be accounted for by a weak electronic coupling constant, V_{CR}, due to the delocalization of the hole over the whole OPE scaffold and to the localization of the electron on a single NDI unit. By contrast, in the NDI/NDI-CSS, both charges are localized on a single NDI and this leads to a much larger V_{CR} provided these NDIs are adjacent.

The exact location of the charges in the CSS is an important parameter that should not be neglected. In the OPE/NDI-CSS, 10 different arrangements of the charges are possible: they correspond to the hole on the OPE and the electron on one of the 10 NDIs. In principle, all 10 arrangements are equivalent and thus their CR dynamics should be essentially the same. The nature of the OPE/NDI-CSS is thus independent of whether it has been populated through OPE (pathway 3) or NDI excitation (pathway 4). As a consequence, the CR dynamics of R10 is independent of the excitation wavelength.

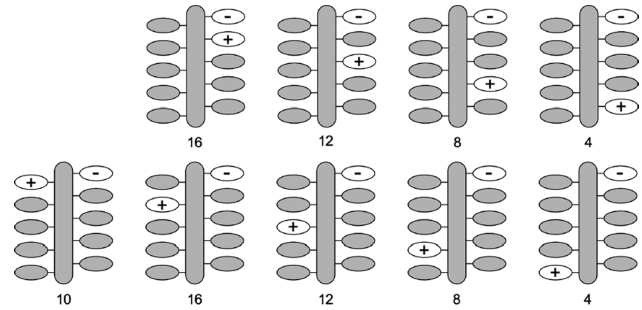

Figure 10. Schematic illustration of the nine nonequivalent arrangements of the charges in an NDI/NDI-CSS. The number of equivalent configurations, in terms of distance between the charges, is written below.

The situation is different with B10, where the charge-separated state is an NDI/NDI-CSS. Indeed in this state, nine nonequivalent arrangements of the charges, over 90 possible ones, have to be considered. These nine configurations, depicted in Figure 10, differ by the number of neutral NDI units intercalated between the charges and by the location of the ionic NDIs on the same side or not of the OPE scaffold. Among these 90 arrangements, 16 are associated with adjacent NDI cation and anion, with a center-to-center distance of about 7−8 Å. CS upon NDI excitation (pathway 5) should exclusively result in such configurations. Other arrangements can subsequently be realized upon hopping of the charges (pathway 8) to other NDIs in competition with CR (pathway 10). However, the short CSS lifetime observed upon NDI excitation of B10 indicates that this competition is in favor of CR.

On the other hand, all 90 possible NDI/NDI-CSS arrangements can be realized upon CS following OPE excitation and hole transfer (pathways 4 and 6). In these other configurations, the center-to-center distance between the ionic NDIs varies from about 15 Å to more than 45 Å, with the largest distance being realized in only four of the 90 arrangements. CR in these states with remote charges can be expected to be extremely slow and thus inoperative. Therefore, the population of these states decays entirely by charge hopping to other configurations until CR eventually takes place through the arrangements with adjacent ionic NDIs. The 3 ns CR component found upon 400 nm excitation of B10 most probably arises from these NDI/NDI-CSS with remote charges. In this case, CR is essentially limited by the diffusion of the charges over the whole molecule. Charge hopping from NDI to NDI can be expected to lead to a decay of the polarization anisotropy of the TA signal. However, transient dichroism measurements did not allow such an effect to be observed as the initial polarization anisotropy of the CSS band upon OPE excitation was too small. This is most probably due to the large number of relative orientations of the NDI units relative to the OPE scaffold. In conclusion, contrary to R10, the CR dynamics of B10 depends on whether the OPE scaffold or an NDI unit is initially excited.

OPE vs POP Scaffold. The CS and CR dynamics of R10 and B10 upon NDI excitation are very similar to those observed with R8 and B8, where the scaffold is a POP.[41] This is not totally surprising as the driving forces for NDI/NDI CS and CR are

the same. Moreover, although the distances between the anchoring positions on the scaffolds are different, both types of systems allow probably enough flexibility for the NDIs to reach similar ranges of distances. The present measurements reveal that the slower CR observed with R10 is due to the involvement of the scaffold as an electron donor. This could not be clearly established with POP because of its absorption below 350 nm. The similar CR dynamics of R10 and R8 can be considered as evidence for POP acting as an electron donor in R8.

The results indicate that using a scaffold with better molecular wire properties than POP apparently does not improve the CSS lifetime. The possible reason is that the effect of the superior hole mobility in OPE is counterbalanced by the smaller driving force for CR by about 0.4 eV. Thus, CR with OPE is less in the inverted regime than with POP.

Despite this, the OPE scaffold offers several important advantages compared to POP. Because of the lower energy of their first electronic transition, OPEs can participate in light harvesting, thus increasing the cross section for absorption in the high frequency region of the visible spectrum. Optical excitation of the scaffold results in an extremely fast CS, because of the large number of quenchers. So fast a CS cannot be realized upon direct NDI excitation. Furthermore, in the case of B10, excitation of the scaffold can result, after CS and hole transfer, in the population of NDI/NDI-CSS with remote ionic units, while direct NDI excitation ends up in states with adjacent ionic units only. Thus, the ability to directly excite the scaffold allows long-lived CSS even if the charges are located on the NDIs.

Concluding Remarks

The results presented here illustrate the remarkable properties of these hybrid multichromophoric systems. Introduction of a chromophoric scaffold opens new charge-separation pathways that are not accessible otherwise. Furthermore, for the blue system, different recombination dynamics are observed although the charges are located on two NDIs in both cases. This is explained by the location of the ionic NDI moieties that depends on the charge separation pathway, hence on the excitation wavelength.

Although very long-lived charge separation is not realized in these systems, several interesting new avenues for ultrafast CS and slow CR can be deduced from the present results. For example, the use of an electron-donating chromophoric scaffold surrounded by many acceptors ensures extremely fast CS. Furthermore, the large delocalization of the hole together with a precise localization of the electron in the resulting CSS guarantees a weak electronic coupling for recombination and thus a relatively long lifetime. Further improvements could probably be achieved with a longer OPE or a similar conjugated oligomeric scaffold. Conjugation in OPE has been shown to saturate at about 10 phenylethynyl units.[69] As many as 20 red NDIs could be attached on such a scaffold. More NDIs would lead to even faster CS and the extended delocalization of the hole to slower recombination.

On the other hand, one way toward long-lived CS with the blue NDIs is to increase the size of the OPE scaffold as well to favor large delocalization of the hole. In this case, the probability for hole transfer to an NDI located far from the $NDI^{\bullet -}$ moiety would be larger than in B10. Recombination could be further reduced by slowing down charge hopping over the NDIs. This could be realized by decreasing the number of NDIs.

A great advantage of such strategies over those mostly pursued until now is the small loss of photonic energy as the dynamics of charge separation and recombination are mostly controlled here by the electronic coupling between the constituents rather than by the driving force. This is of course a crucial parameter for the design of efficient photoactive systems.

Acknowledgment. The authors wish to thank the Swiss National Science Foundation for financial support.

References and Notes

(1) Gust, D.; Moore, T. A.; Moore, A. L. *Acc. Chem. Res.* **1993**, *26*, 198.
(2) Gust, D.; Moore, T. A.; Moore, A. L.; Macpherson, A. N.; Lopez, A.; DeGraziano, J. M.; Gouni, I.; Bittersmann, E.; Seely, G. R.; et al. *J. Am. Chem. Soc.* **1993**, *115*, 11141–11152.
(3) Guldi, D. M.; Imahori, H.; Tamaki, K.; Kashiwagi, Y.; Yamada, H.; Sakata, Y.; Fukuzumi, S. *J. Phys. Chem. A* **2004**, *108*, 541–548.
(4) Borgstroem, M.; Shaikh, N.; Johansson, O.; Anderlund, M. F.; Styring, S.; Aakermark, B.; Magnuson, A.; Hammarstroem, L. *J. Am. Chem. Soc.* **2005**, *127*, 17504–17515.
(5) Ohkubo, K.; Kotani, H.; Shao, J.; Ou, Z.; Kadish, K. M.; Li, G.; Pandey, R. K.; Fujitsuka, M.; Ito, O.; Imahori, H.; Fukuzumi, S. *Angew. Chem., Int. Ed.* **2004**, *43*, 853–856.
(6) Han, Y.; Dobeck, L.; Gong, A.; Meng, F.; Spangler, C. W.; Spangler, L. H. *Chem. Commun.* **2005**, 1067–1069.
(7) Guldi, D. M. *Chem. Soc. Rev.* **2002**, *31*, 22–36.
(8) D'Souza, F.; Smith, P. M.; Zandler, M. E.; McCarty, A. L.; Itou, M.; Araki, Y.; Ito, O. *J. Am. Chem. Soc.* **2004**, *126*, 7898–7907.
(9) Kodis, G.; Terazono, Y.; Liddell, P. A.; Andréasson, J.; Garg, V.; Hambourger, M.; Moore, T. A.; Moore, A. L.; Gust, D. *J. Am. Chem. Soc.* **2006**, *128*, 1818.
(10) D'Souza, F.; Gadde, S.; Islam, D. M. S.; Wijesinghe, C. A.; Schumacher, A. L.; Zandler, M. E.; Araki, Y.; Ito, O. *J. Phys. Chem. A* **2007**, *111*, 8552–8560.
(11) Wurthner, F.; Chen, Z.; Hoeben, F. J. M.; Osswald, P.; You, C. C.; Jonkheijm, P.; Herrikhuyzen, J. v.; Schenning, A. P. H. J.; vanderSchoot, P. P. A. M.; Meijer, E. W.; Beckers, E. H. A.; Meskers, S. C. J.; Janssen, R. A. J. *J. Am. Chem. Soc.* **2004**, *126*, 10611–10618.
(12) Yamamoto, Y.; Fukushima, T.; Suna, Y.; Ishii, N.; Saeki, A.; Seki, S.; Tagawa, S.; Masateru, T.; Kawai, T.; Aida, T. *Science* **2006**, *314*, 1761–1764.
(13) Ohkubo, K.; Sintic, P. J.; Tkachenko, N. V.; Lemmetyinen, H.; E, W.; Ou, Z.; Shao, J.; Kadish, K. M.; Crossley, M. J.; Fukuzumi, S. *Chem. Phys.* **2006**, *326*, 3–14.
(14) Bhosale, S.; Sisson, A. L.; Talukdar, P.; Fürstenberg, A.; Banerji, N.; Vauthey, E.; Bollot, G.; Mareda, J.; Röger, C.; Würthner, F.; Sakai, N.; Matile, S. *Science* **2006**, *313*, 84.
(15) Wasielewski, M. R. *J. Org. Chem.* **2006**, *71*, 5051–5066.
(16) Sakai, N.; Sisson, A. L.; Bhosale, S.; Fürstenberg, A.; Banerji, N.; Vauthey, E.; Matile, S. *Org. Biomol. Chem.* **2007**, *5*, 2560–2563.
(17) Sakai, N.; Sisson, A. L.; Bürgi, T.; Matile, S. *J. Am. Chem. Soc.* **2007**, *129*, 15758–15759.
(18) Sisson, A. L.; Sakai, N.; Banerji, N.; Fürstenberg, A.; Vauthey, E.; Matile, S. *Angew. Chem., Int. Ed.* **2008**, *47*, 3727–3729.
(19) Kim, O.-K.; Melinger, J.; Chung, S.-J.; Pepitone, M. *Org. Lett.* **2008**, *10*, 1625–1628.
(20) Fleming, G. R.; VanGrondelle, R. *Curr. Opin. Struct. Biol.* **1997**, *7*, 738.
(21) Sundström, V.; Pullerits, T.; van Grondelle, R. *J. Phys. Chem. B* **1999**, *103*, 2327–2346.
(22) van Amerongen, H.; Valkunas, L.; van Grondelle, R. *Photosynthetic Excitons*; World Scientific: Singapore, 2000.
(23) Biemans, H. A. M.; Rowan, A. E.; Verhoeven, A.; Vanoppen, P.; Latterini, L.; Foekema, J.; Schenning, A. P. H. J.; Meijer, E. W.; deSchryver, F. C.; Nolte, R. J. M. *J. Am. Chem. Soc.* **1998**, *120*, 11054.
(24) Brodard, P.; Matzinger, S.; Vauthey, E.; Mongin, O.; Papamicaël, C.; Gossauer, A. *J. Phys. Chem. A* **1999**, *103*, 5858.
(25) Yeow, E. K. L.; Ghiggino, K. P.; Reek, J. N. H.; Crossley, M. J.; Bosman, A. W.; Schenning, A. P. H. J.; Meijer, E. W. *J. Phys. Chem. B* **2000**, *104*, 2596–2606.
(26) Holten, D.; Bocian, D. F.; Lindsey, J. S. *Acc. Chem. Res.* **2002**, *35*, 57.
(27) Aratani, N.; Osuka, A.; Cho, H. S.; Kim, D. *J. Photochem. Photobiol., C* **2002**, *3*, 25–52.
(28) Imahori, H. *J. Phys. Chem. B* **2004**, *108*, 6130.
(29) Morandeira, A.; Vauthey, E.; Schuwey, A.; Gossauer, A. *J. Phys. Chem. A* **2004**, *108*, 5741–5751.
(30) Rhee, H.; Joo, T.; Aratani, N.; Osuka, A.; Cho, S.; Kim, D. *J. Chem. Phys.* **2006**, *125*, 074902.
(31) Berberan-Santos, M. N.; Choppinet, P.; Fedorov, A.; Jullien, L.; Valeur, B. *J. Am. Chem. Soc.* **1999**, *121*, 2526–2533.

(32) Rybtchinski, B.; Sinks, L. E.; Wasielewski, M. R. *J. Am. Chem. Soc.* **2004**, *126*, 12268–12269.
(33) Ziessel, R.; Goze, C.; Ulrich, G.; Cesario, M.; Retailleau, P.; Harriman, A.; Rostron, J. P. *Chem.—Eur. J.* **2005**, *11*, 7366–7378.
(34) Sautter, A.; Kaletas, B. K.; Schmid, D. G.; Dobrawa, R.; Zimine, M.; Jung, G.; Van Stokkum, I. H. M.; De Cola, L.; Williams, R. M.; Wuerthner, F. *J. Am. Chem. Soc.* **2005**, *127*, 6719–6729.
(35) You, C.-C.; Hippius, C.; Gruene, M.; Wuerthner, F. *Chem.—Eur. J.* **2006**, *12*, 7510–7519.
(36) Becker, K.; Lagoudakis, P. G.; Gaefke, G.; Hoeger, S.; Lupton, J. M. *Angew. Chem., Int. Ed.* **2007**, *46*, 3450–3455.
(37) Oesterling, I.; Muellen, K. *J. Am. Chem. Soc.* **2007**, *129*, 4595–4605.
(38) Devadoss, C.; Bharathi, P.; Moore, J. S. *J. Am. Chem. Soc.* **1996**, *118*, 9635.
(39) Kopelman, R.; Shortreed, M.; Shi, Z.-Y.; Tan, W.; Xu, Z.; Moore, J. S.; Bar-Haim, A.; Klafter, J. *Phys. Rev. Lett.* **1997**, *78*, 1239–1242.
(40) Kleiman, V. D.; Melinger, J. S.; McMorrow, D. *J. Phys. Chem. B* **2001**, *105*, 5595–5598.
(41) Banerji, N.; Fürstenberg, A.; Bhosale, S.; Sisson, A. L.; Sakai, N.; Matile, S.; Vauthey, E. *J. Phys. Chem. B* **2008**, *112*, 8912–8922.
(42) Giesa, R. *J. Macromol. Sci. Rev. Macromol. Chem. Phys.* **1996**, *C36*, 631–670.
(43) Bunz, U. H. F. *Chem. Rev.* **2000**, *100*, 1605–1644.
(44) Tour, J. M. *Acc. Chem. Res.* **2000**, *33*, 791–804.
(45) Fürstenberg, A.; Julliard, M. D.; Deligeorgiev, T. G.; Gadjev, N. I.; Vassilev, A. A.; Vauthey, E. *J. Am. Chem. Soc.* **2006**, *128*, 7661–7669.
(46) Morandeira, A.; Engeli, L.; Vauthey, E. *J. Phys. Chem. A* **2002**, *106*, 4833–4837.
(47) Duvanel, G.; Banerji, N.; Vauthey, E. *J. Phys. Chem. A* **2007**, *111*, 5361–5369.
(48) Würthner, F.; Shahadat, A.; Thalacker, C.; Debaerdemaeker, T. *Chem.—Eur. J.* **2002**, *8*, 4742.
(49) Duvanel, G.; Grilj, J.; Schuwey, A.; Gossauer, A.; Vauthey, E. *Photochem. Photobiol. Sci.* **2007**, *6*, 956–963.
(50) Sluch, M. I.; Godt, A.; Bunz, U. H. F.; Berg, M. A. *J. Am. Chem. Soc.* **2001**, *123*, 6447–6448.
(51) Barros, T. C.; Brochsztain, S.; Toscano, V. G.; Berci Filho, P.; Politi, M. J. *J. Photochem. Photobiol., A* **1997**, *111*, 97–104.
(52) Alp, S.; Erten, S.; Karapire, C.; Koz, B.; Doroshenko, A. O.; Icli, S. *J. Photochem. Photobiol., A* **2000**, *135*, 103–110.
(53) Sudeep, P. K.; James, P. V.; Thomas, K. G.; Kamat, P. V. *J. Phys. Chem. A* **2006**, *110*, 5642–5649.
(54) Hu, W.; Zhu, N.; Tang, W.; Zhao, D. *Org. Lett.* **2008**, *10*, 2669–2672.
(55) Kasha, M.; Rawls, H. R.; El-Bayoumi, M. A. *Pure Appl. Chem.* **1965**, *11*, 371–392.
(56) Fürstenberg, A., PhD Thesis, University of Geneva, 2008.
(57) Fleming, G. R. *Chemical Applications of Ultrafast Spectroscopy*; Oxford University Press: New York, 1986.
(58) Vauthey, E. *Chem. Phys. Lett.* **1993**, *216*, 530–536.
(59) Rehm, D.; Weller, A. *Isr. J. Chem.* **1970**, *8*, 259–271.
(60) Kel, O.; Grilj, J.; Sakai, N.; Matile, S.; Vauthey, E. To be published.
(61) Siemiarczuk, A.; Wagner, B. D.; Ware, W. R. *J. Phys. Chem.* **1990**, *94*, 1661–1666.
(62) Clifford, J. N.; Gu, T.; Nierengarten, J.-F.; Armaroli, N. *Photochem. Photobiol. Sci.* **2006**, *5*, 1165–1172.
(63) Marcus, R. A.; Sutin, N. *Biochim. Biophys. Acta* **1985**, *811*, 265–322.
(64) Fuller, M. J.; Gusev, A. V.; Wasielewski, M. R. *Isr. J. Chem.* **2004**, *44*, 101–108.
(65) Fuller, M. J.; Sinks, L. E.; Rybtchinksi, B.; Giaimo, J. M.; Li, X.; Wasielewski, M. R. *J. Phys. Chem. A* **2005**, *109*, 970.
(66) Gadonas, R.; Feller, K.-H.; Pugzlys, A.; Jonusauskas, G.; Oberlé, J.; Rullière, C. *J. Chem. Phys.* **1997**, *106*, 8374.
(67) Valeur, B. *Molecular Fluorescence. Principles and Applications*; Wiley-VCH: Weinheim, 2001; p 172.
(68) Lakowicz, J. R. *Principles of Fluorescence Spectroscopy*, 3rd ed.; Springer: New York, 2006; p 142.
(69) Meier, H.; Ickenroth, D.; Stalmach, U.; Koynooov, K.; Bahtiar, A.; Bubeck, C. *Eur. J. Org. Chem.* **2001**, 4431–4443.

JP903572R